A perturbation method for evaluating nonlinear normal modes of a piecewise linear two degree of freedom system

Fabrizio Vestroni, Achille Paolone, Angelo Luongo

A perturbation method for evaluating nonlinear normal modes of a piecewise linear two-degrees-of-freedom system

Fabrizio Vestroni · Angelo Luongo · Achille Paolone

Abstract The classical Lindstedt–Poincaré method is adapted to analyze the nonlinear normal modes of a piecewise linear system. A simple two degrees-of-freedom, representing a beam with a breathing crack is considered. The fundamental branches of the two modes and their stability are drawn by varying the severity of the crack, i.e., the level of nonlinearity. Results furnished by the asymptotic method give insight into the mechanical behavior of the system and agree well with numerical results; the existence of superabundant modes is proven. The unstable regions and the bifurcated branches are followed by a numerical procedure based on the Poincarè map.

Keywords Nonlinear normal modes · Piecewise-linear systems · Perturbation methods · Damaged systems · Cracked beams

1 Introduction

The linear dynamics of multi-degree-of-freedom (or continuous) systems are governed by their natural frequencies and modes. The concept of normal mode was generalized to nonlinear systems by Rosemberg [1–3], however, the original definition has been modified over the years. Shaw and Pierre [4–6] extended the concept of nonlinear normal modes (NNMs) to systems affected by damping and gyroscopic forces, but limited their analysis to solutions close to the linear ones. The issue has been extensively covered by many researchers [7–11]. Most of the results are devoted to analyzing the modification of the linear modes with the oscillation amplitude, and are generally tackled via asymptotic methods (see [12] for an overview, and [13, 14] for a multiple scale analysis).

For weak nonlinear motions, NNMs are close to linear modes and of the equal number. They constitute a base in which computationally efficient reduced-order models are built-up. However, for strong nonlinear motions, the occurrence of superabundant modes is observed, generated by bifurcation mechanisms [3, 15–18]. The interest in the existence of such modes is related to the existence of extra-peaks in the frequency response function, leading to new attractive phenomena, such as unexpected resonances, localization, and energy transfer [17, 19, 20]. While the Rosemberg approach is able to identify these bifurcated solutions to the authors' knowledge, the applicability of asymptotic methods has not been investigated yet.

The occurrence of novel modes is notably governed by the amount of the nonlinear part of the equation of motion [16]. Superabundant modes have been ob-

F. Vestroni · A. Paolone (✉)
DISG, University of Rome "La Sapienza", via Eudossiana, 18, 00184 Rome, Italy
e-mail: achille.paolone@uniroma1.it

A. Luongo
DISAT, University of L'Aquila, Monteluco di Roio, 67040 L'Aquila, Italy

served in smooth systems only under particular circumstances [8, 15]. They are more likely to appear in nonsmooth systems [21, 22], as those possessing discontinuous restoring forces [23–27].

The aim of this paper is to investigate the dynamics of systems expected to exhibit superabundant modes. An important example of piecewise smooth system (PSS) is considered, as a beam with a breathing crack by taking advantage of related works present in literature [23, 28–30]. For this system, the phase-space consists of two regions separated by a surface at which the vector field is continuous while the Jacobian is discontinuous. As major novelty of the approach followed here, the Lindstedt–Poincarè method is applied under the hypothesis the discontinuity is small. In other words, the nondifferentiable part (nonsmoothness) of the equation of motion is assumed as a perturbation of a generating linear (i.e., smooth) system. In spite of this apparently strong limitation, numerical results show that the asymptotic solution truncated at the second order works well also for considerably large discontinuities. Although the asymptotic analysis is limited to the fundamental solutions and their stability, it clarifies the main peculiar aspects of the nonlinear modal characteristics of the PSS considered. It also furnishes a frame for a global analysis, performed by a numerical approach based on the Poincaré map, used here only to describe the bifurcated NNMs.

2 Two-degrees-of-freedom model

In order to illustrate the method, a simple two-degrees-of-freedom model is considered, coarsely modeling a flexible cracked beam. It consists of a double pendulum (Fig. 1a) with two lumped masses, m_i $(i = 1, 2)$, located at the endpoints of two massless rigid rods. A linear rotational spring of constant k_1 connects the first rod to the ground, while a piecewise linear rotational spring connects the two rods. The model is only a small refinement of that studied in [23]. By assuming the rotations q_1 and q_2 as Lagrangian coordinates (Fig. 1a), the constitutive law of the internal nonlinear rotational spring reads:

$$M_2 = \begin{cases} k_2(1-\varepsilon)\eta & \text{if } \eta > 0, \\ k_2\eta & \text{if } \eta \le 0 \end{cases} \tag{1}$$

or, equivalently:

$$M_2 = k_2\big(1 - \varepsilon H[\eta]\big)\eta \tag{2}$$

where M_2 is the internal piecewise linear moment (Fig. 1b), k_2 is the undamaged stiffness, ε is the damage parameter, equal to the relative jump in the piecewise constant rotational stiffness (Fig. 1c), H is the Heaviside function and η is the relative rotation between the two bars, i.e., $\eta = q_2 - q_1$. Since

$$\eta = \mathbf{a}^T\mathbf{q} \tag{3}$$

with $\mathbf{a} = (-1,\ 1)^T$ and $\mathbf{q} = (q_1,\ q_2)^T$, $\mathbf{a}$ is a vector in the configuration space $\{q_i\}$ $(i = 1, 2)$, normal to the

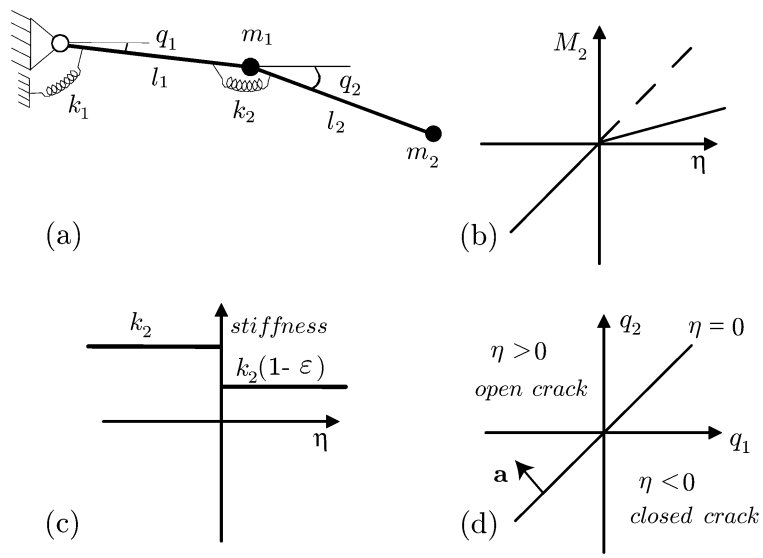

Fig. 1 (**a**) Mechanical model and Lagrangian parameters; (**b**) piecewise linear moment; (**c**) piecewise constant rotational stiffness; (**d**) configuration space

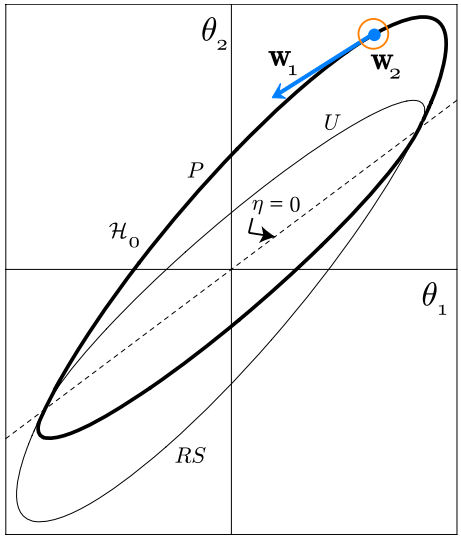

Fig. 2 Isoenergetic curves of the undamaged (U), reduced stiffness (RS) and piecewise (P) system

straight line for the origin that separates states in which the crack is open from states in which it is closed (Fig. 1d).

Using the notations of Fig. 1, the following dimensional equations of motion are found:

$$\begin{aligned}&(m_1+m_2)l_1^2\ddot{q}_1+m_2l_1l_2\ddot{q}_2+\big[k_1+k_2\big(1-\varepsilon H[\eta]\big)\big]q_1\\&\quad-k_2\big(1-\varepsilon H[\eta]\big)q_2=0,\\&m_2l_1l_2\ddot{q}_1+m_2l_2^2\ddot{q}_2-k_2\big(1-\varepsilon H[\eta]\big)q_1\\&\quad+k_2\big(1-\varepsilon H[\eta]\big)q_2=0\end{aligned}\tag{4}$$

where dots denote differentiation with respect to time t. By letting $L=l_1+l_2$ and $M=m_1+m_2$, and introducing the following dimensionless quantities:

$$\tilde{m}_i=\frac{m_i}{M},\qquad \tilde{l}_i=\frac{l_i}{L},\qquad \tilde{k}_i=\frac{k_i}{k_1},\quad i=1,2\tag{5}$$

the equations of motion (4) are rewritten in nondimensional form:

$$\mathbf{M}\ddot{\mathbf{q}}+\big(\mathbf{K}_0-\varepsilon H[\eta]\mathbf{K}_2\big)\mathbf{q}=\mathbf{0}\tag{6}$$

where dots now denote differentiation with respect to the dimensionless time $\tilde{t}:=(k_1/ML^2)^{1/2}t$, and:

$$\begin{aligned}\mathbf{M}&=\begin{bmatrix}\tilde{l}_1^2 & \tilde{m}_2\tilde{l}_1\tilde{l}_2\\ \tilde{m}_2\tilde{l}_1\tilde{l}_2 & \tilde{m}_2\tilde{l}_2^2\end{bmatrix},\\ \mathbf{K}_0&=\begin{bmatrix}1+\tilde{k}_2 & -\tilde{k}_2\\ -\tilde{k}_2 & \tilde{k}_2\end{bmatrix},\\ \mathbf{K}_2&=\tilde{k}_2\begin{bmatrix}1 & -1\\ -1 & 1\end{bmatrix}.\end{aligned}\tag{7}$$

3 Asymptotic solution: the Lindstedt–Poincarè method

Equations (6) are solved asymptotically for small values of the damage parameter, $\varepsilon\ll 1$. The undamaged ($\varepsilon=0$) system admits 2 eigenpairs $(\omega_x,\mathbf{u}_x)$, $(\omega_y,\mathbf{u}_y)$ so that

$$\mathbf{K}_0\mathbf{u}_\alpha-\omega_\alpha^2\mathbf{M}\mathbf{u}_\alpha=\mathbf{0},\quad \alpha=x,y.\tag{8}$$

The modal matrix of the undamaged system is used to perform a transformation to normal coordinates. Putting $\mathbf{q}=x\mathbf{u}_x+y\mathbf{u}_y$, (6) become

$$\begin{aligned}&\ddot{x}+\omega_x^2x-\varepsilon H[\eta]\big(c_{xx}x+c_{xy}y\big)=0,\\&\ddot{y}+\omega_y^2y-\varepsilon H[\eta]\big(c_{yx}x+c_{yy}y\big)=0\end{aligned}\tag{9}$$

where $c_{\alpha\beta}:=\mathbf{u}_\alpha^T\mathbf{K}_2\mathbf{u}_\beta$, $(\alpha,\beta)=(x,y)$.

The modifications of individual modes are studied separately; the nonlinear normal mode of the damaged ($\varepsilon\neq 0$) system, close to the linear eigenvector $\mathbf{u}_x$ is sought. Consequently, the x is referred to as an *active* coordinate, while the y is called a *passive* coordinate; to obtain the other nonlinear normal mode, x and y must be interchanged. The Lindstedt–Poincarè technique is applied to the nonlinear, nonsmooth equations of motion, by letting:

$$\theta=\Omega_x t,\quad \Omega_x=\omega_x\big(1+\varepsilon\mu_1+\varepsilon^2\mu_2+\cdots\big)\tag{10}$$

where Ω_x is the unknown nonlinear frequency and μ_i's are frequency corrections to be determined. The modal coordinates are expanded in series of ε:

$$\begin{pmatrix}x\\y\end{pmatrix}=\begin{pmatrix}x_0\\0\end{pmatrix}+\varepsilon\begin{pmatrix}x_1\\y_1\end{pmatrix}+\varepsilon^2\begin{pmatrix}x_2\\y_2\end{pmatrix}+\cdots.\tag{11}$$

Since $\eta = \eta(\varepsilon)$, the Heaviside function appearing in the equation of motion admits the generalized power series:

$$H\big[\eta(\varepsilon)\big] = H[\eta_0] + \delta[\eta_0]\big(\varepsilon\eta_1 + \varepsilon^2\eta_2 + \cdots\big) + \frac{1}{2}\delta'[\eta_0]\big(\varepsilon^2\eta_1^2 + \cdots\big) \tag{12}$$

where δ is the Dirac function and $\eta_j = \mathbf{a}^T(\mathbf{u}_x x_j + \mathbf{u}_y y_j)$ $(j = 0, 1, \ldots)$. Previous expansions and the chain rule lead to the following perturbation equations:

$$\varepsilon^0 : \Big\{\omega_x^2\,(\ddot{x}_0 + x_0) = 0,$$

$$\varepsilon^1 : \begin{cases} \omega_x^2(\ddot{x}_1 + x_1) = H[\eta_0]c_{xx}x_0 - 2\omega_x^2\mu_1\ddot{x}_0, \\ \omega_x^2(\ddot{y}_1 + \lambda^2 y_1) = H[\eta_0]c_{yx}x_0, \end{cases}$$

$$\varepsilon^2 : \begin{cases} \omega_x^2(\ddot{x}_2 + x_2) \\ \quad = H[\eta_0](c_{xx}x_1 + c_{xy}y_1) - \omega_x^2(2\mu_2 + \mu_1^2)\ddot{x}_0 \\ \quad\quad - 2\mu_1\omega_x^2\ddot{x}_1 + \delta[\eta_0]\eta_1 c_{xx}x_0, \\ \omega_x^2(\ddot{y}_2 + \lambda^2 y_2) \\ \quad = H[\eta_0](c_{yx}x_1 + c_{yy}y_1) - 2\mu_1\omega_x^2\ddot{y}_1 \\ \quad\quad + \delta[\eta_0]\eta_1 c_{yx}x_0 \end{cases} \tag{13}$$

where $\lambda = \omega_y/\omega_x$. These equations must be integrated together with the 2π-*periodicity conditions* on the θ-scale:

$$\xi_i(-\pi) = \xi_i(\pi), \qquad \dot{\xi}_i(-\pi) = \dot{\xi}_i(\pi), \quad \xi = x, y, \quad i = 0, 1, 2, \ldots. \tag{14}$$

The ε^0-order equation admits the periodic (generating) solution:

$$x_0 = a\sin\theta, \quad \theta \in [-\pi, \pi] \tag{15}$$

where a is the amplitude and the inessential initial phase has been taken equal to zero, since the system is autonomous. By normalizing the $\mathbf{u}_x$ eigenvector in such a way that $\mathbf{a}^T\mathbf{u}_x > 0$, it follows that $\eta_0 > 0$ when $\theta \in (0, \pi)$, $\eta_0 < 0$ when $\theta \in (-\pi, 0)$ and $\eta_0 = 0$ when $\theta \equiv (-\pi, 0, \pi)$; therefore, in the higher-order perturbation equations:

$$H[\eta_0] \equiv W[0, \pi] \tag{16}$$

where $W[0, \pi] = H[\theta] - H[\theta - \pi]$. Moreover, up-to the ε^2-order, neither δ nor its derivatives furnish contribution to the perturbation solution, according to definition of the Dirac function. A brief sketch on how to deal, at higher orders, with perturbation equations containing such a generalized function is given in Appendix A.

The ε^2- and ε^3-order equations govern the motion of a linear *smooth* system (namely, the undamaged one), subjected to a *nonsmooth* or *discontinuous* excitation. They are of the following type:

$$\omega_x^2(\ddot{x}_i + x_i) = \begin{cases} F_i^+(\theta), & \theta \in (0, \pi], \\ F_i^-(\theta), & \theta \in [-\pi, 0), \end{cases}$$
$$\omega_x^2\big(\ddot{y}_i + \lambda^2 y_i\big) = \begin{cases} G_i^+(\theta), & \theta \in (0, \pi], \\ G_i^-(\theta), & \theta \in [-\pi, 0), \end{cases} \quad i = 1, 2 \tag{17}$$

where $F_i^{\pm}(\theta)$ and $G_i^{\pm}(\theta)$ are smooth laws. By denoting by $\xi_i^+(\theta)$ and $\xi_i^-(\theta)$ $(\xi = x, y)$, the relevant responses, *continuity* requires that:

$$\xi_i^-(0) = \xi_i^+(0), \qquad \dot{\xi}_i^-(0) = \dot{\xi}_i^+(0), \quad i = 1, 2 \tag{18}$$

and *periodicity* calls for:

$$\xi_i^-(-\pi) = \xi_i^+(\pi), \qquad \dot{\xi}_i^-(-\pi) = \dot{\xi}_i^+(\pi), \quad i = 1, 2. \tag{19}$$

All these prescriptions will be referred to in the following as "boundary conditions".

3.1 First-order solution

Substitution of (15) into (13_2) leads to:

$$\ddot{x}_1 + x_1 = \begin{cases} \frac{ac_{xx}\sin\theta}{\omega_x^2} + 2a\mu_1\sin\theta, & \theta \in [0, \pi], \\ 2a\mu_1\sin\theta, & \theta \in [-\pi, 0], \end{cases}$$
$$\ddot{y}_1 + \lambda^2 y_1 = \begin{cases} \frac{ac_{yx}\sin\theta}{\omega_x^2}, & \theta \in [0, \pi], \\ 0, & \theta \in [-\pi, 0]. \end{cases} \tag{20}$$

The right-hand members of (20), $F_1(\theta)$ and $G_1(\theta)$ are plotted in the upper part of Fig. 3 for the sample system described in Sect. 4, and for the first and second modes. The graphs differ only in a scaling factor, showing that nonlinearities are higher in the second mode. Under the assumption that *no internal resonance* occurs, namely $\lambda \neq 1$, the following solution

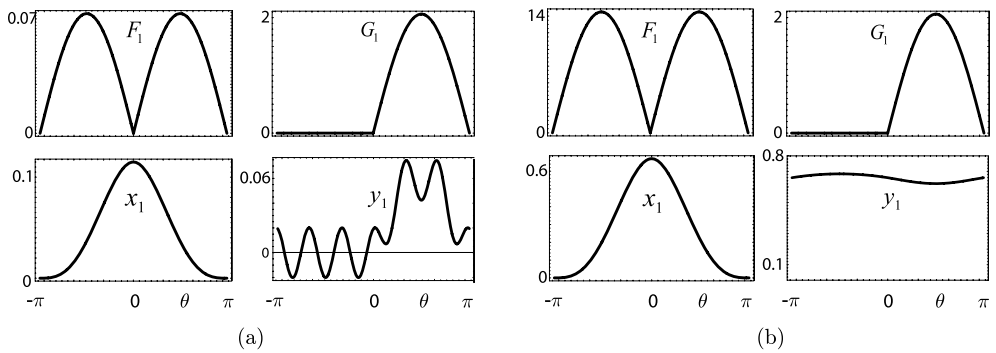

Fig. 3 Nonsmooth excitations of the first-order perturbation equations (20) and relevant responses; (**a**) first mode; (**b**) second mode

is found:

$$x_1 = \begin{cases} A_1^+ \cos\theta + B_1^+ \sin\theta - (\frac{c_{xx}}{2\omega_x^2} + \mu_1) a\theta \cos\theta, \\ \quad \theta \in [0, \pi], \\ A_1^- \cos\theta + B_1^- \sin\theta - \mu_1 a\theta \cos\theta, \\ \quad \theta \in [-\pi, 0], \end{cases}$$
$$y_1 = \begin{cases} C_1^+ \cos(\lambda\theta) + D_1^+ \sin(\lambda\theta) + \frac{a c_{yx} \sin\theta}{(\lambda^2 - 1)\omega_x^2}, \\ \quad \theta \in [0, \pi], \\ C_1^- \cos(\lambda\theta) + D_1^- \sin(\lambda\theta), \\ \quad \theta \in [-\pi, 0], \end{cases} \tag{21}$$

where A's, B's, C's and D's are arbitrary constants. It is worth noting that such constants *must be introduced* to satisfy the boundary conditions, in contrast to the usual applications of the Lindstedt–Poincaré method for smooth systems, where the C_1's and D_1's constants *must be ignored*, in order to avoid the destruction of the 2π-periodicity by the incommensurable frequency λ. The x-coordinate is considered first. By requiring:

$$\begin{aligned} &x_1^-(0) = x_1^+(0), \qquad \dot{x}_1^-(0) = \dot{x}_1^+(0), \\ &x_1^-(-\pi) = x_1^+(\pi), \qquad \dot{x}_1^-(-\pi) = \dot{x}_1^+(\pi) \end{aligned} \tag{22}$$

the following system in the $A_1^{\pm}$, $B_1^{\pm}$ constants is found:

$$\begin{bmatrix} 1 & 0 & -1 & 0 \\ 0 & 1 & 0 & -1 \\ 1 & 0 & -1 & 0 \\ 0 & 1 & 0 & -1 \end{bmatrix} \begin{pmatrix} A_1^+ \\ B_1^+ \\ A_1^- \\ B_1^- \end{pmatrix}$$
$$= \frac{1}{2\omega_x^2} \begin{pmatrix} 0 \\ c_{xx} + \mu_1 \omega_x^2 \\ \pi \left(c_{xx} + 4\mu_1 \omega_x^2 \right) \\ c_{xx} + \mu_1 \omega_x^2 \end{pmatrix}, \tag{23}$$

The matrix is singular, since the associate homogeneous problem of the undamaged case admits the nontrivial independent solutions, $A_1^+ = A_1^-$ and $B_1^+ = B_1^-$, corresponding to free motions in the x-mode (this, indeed, satisfies 2π-periodicity and continuity). Therefore, for solvability, the known term must be in the range of the matrix. The two conditions of orthogonality to the eigensolutions of the transpose problem degenerate in a unique (solvability) condition, from which the first frequency correction μ_1 is drawn:

$$\mu_1 = -\frac{c_{xx}}{4\omega_x^2}. \tag{24}$$

Two out of four constants $A_1^{\pm}$, $B_1^{\pm}$, however, remain indeterminate and can be chosen through somewhat arbitrary normalization conditions. Here the following normalization:

$$x_1^+(\pi) = 0, \qquad \dot{x}_1^+(\pi) = 0 \tag{25}$$

is adopted, from which:

$$A_1^+ = A_1^- = \frac{a c_{xx} \pi}{4\omega_x^2}; \qquad B_1^+ = -B_1^- = \frac{a c_{xx}}{4\omega_x^2} \tag{26}$$

is obtained. The responses (21) are plotted in the bottom part of Fig. 3.

As an alternative to the procedure illustrated, and similarly to the classical Lindstedt–Poincarè approach to the smooth systems, one can recognize the need to

remove the resonance between the 2π-periodic piecewise forcing and the x-mode, of the same period. We avoid the usual locution "removing secular terms", which in contrast, *do appear* in the $x_1^{\pm}(\theta)$ laws, and which do not diverge to infinity, since they are defined in the finite intervals $[-\pi, 0]$, $[0, \pi]$. According to this procedure, the following orthogonality conditions must hold:

$$\left(\frac{ac_{xx}\sin\theta}{\omega_x^2} + 2a\mu_1\sin\theta\right)a\int_0^{\pi}\sin^2\theta\,d\theta + 2a^2\mu_1\sin\theta\int_{-\pi}^{0}\sin^2\theta\,d\theta = 0 \tag{27}$$

thus, suppressing the forcing fundamental harmonic on the x-mode. If this approach is followed, the periodicity conditions on $x(\theta)$ are automatically satisfied, as a consequence of the periodicity of the forcing and removing resonance, so that only continuity must be enforced.

Moving to the passive y-coordinate, the boundary conditions are imposed by requiring:

$$\begin{aligned} &y_1^-(0) = y_1^+(0), \qquad \dot{y}_1^-(0) = \dot{y}_1^+(0),\\ &y_1^-(-\pi) = y_1^+(\pi), \qquad \dot{y}_1^-(-\pi) = \dot{y}_1^+(\pi) \end{aligned} \tag{28}$$

and the following system in the $C_1^{\pm}$, $D_1^{\pm}$ constants is found:

$$\begin{bmatrix} 1 & 0 & -1 & 0\\ 0 & \lambda & 0 & -\lambda\\ c(\pi\lambda) & s(\pi\lambda) & -c(\pi\lambda) & s(\pi\lambda)\\ -\lambda s(\pi\lambda) & \lambda c(\pi\lambda) & -\lambda s(\pi\lambda) & -\lambda c(\pi\lambda) \end{bmatrix} \times \begin{pmatrix} C_1^+\\ D_1^+\\ C_1^-\\ D_1^- \end{pmatrix} = \frac{ac_{yx}}{\omega_x^2(\lambda^2-1)}\begin{pmatrix} 0\\ -1\\ 0\\ 1 \end{pmatrix} \tag{29}$$

where c and s denote cosine and sine functions, respectively. Differently from the active variable, *the matrix is nonsingular*. In fact, the undamaged system does not admit 2π-periodic motions in the y-coordinate, since $\lambda \neq 1$. Forcing terms, however, make the y-response 2π-periodic, if the previous equations are satisfied. By solving them, *a unique solution* is found:

$$\begin{aligned} C_1^+ &= C_1^- = \frac{ac_{xy}\cot(\pi\lambda/2)}{2\lambda(1-\lambda^2)\omega_x^2},\\ D_1^+ &= -D_1^- = \frac{ac_{xy}}{2\lambda(1-\lambda^2)\omega_x^2}. \end{aligned} \tag{30}$$

3.2 Second-order solution

The ε^2-order perturbation equations can be dealt with as previously illustrated. Taking into account equations (26)–(30), substitution of (15) and (21) into (13_3) leads to:

$$\omega_x^2(\ddot{x}_2 + x_2) = \begin{cases} \frac{1}{\omega_x^2}[c_{xx}x_1 + c_{xy}y_1 - \omega_x^2(2\mu_2+\mu_1^2)\ddot{x}_0 - 2\mu_1\omega_x^2\ddot{x}_1], & \theta\in[0,\pi],\\ \frac{1}{\omega_x^2}[-\omega_x^2(2\mu_2+\mu_1^2)\ddot{x}_0 - 2\mu_1\omega_x^2\ddot{x}_1], & \theta\in[-\pi,0], \end{cases}$$

$$\omega_1^2(\ddot{y}_2 + \lambda^2 y_2) = \begin{cases} c_{xy}x_1 + c_{yy}y_1 - 2\mu_1\omega_x\ddot{y}_1, & \theta\in[0,\pi],\\ -2\mu_1\omega_x\ddot{y}_1, & \theta\in[-\pi,0]. \end{cases} \tag{31}$$

By requiring that the r.h.m. of (31_1) be orthogonal to the generating solution, we have the following:

$$-2\mu_1\omega_x^2\int_{-\pi}^{\pi}\ddot{x}_1\sin\theta\,d\theta + \omega_x^2(2\mu_2+\mu_1^2)a\int_{-\pi}^{\pi}\sin^2\theta\,d\theta + \int_0^{\pi}(c_{xx}x_1 + c_{xy}y_1)\sin\theta\,d\theta = 0. \tag{32}$$

By substituting $x_1(\theta)$ in the integral and performing time integrations, the second-order frequency correction is obtained as:

$$\mu_2 = \frac{\pi\lambda(\lambda^2-1)[2c_{xy}^2 + c_{xx}^2(\lambda^2-1)] + 4c_{xy}\cot(\pi\lambda/2)}{8\pi\lambda(\lambda^2-1)\omega_x^4}. \tag{33}$$

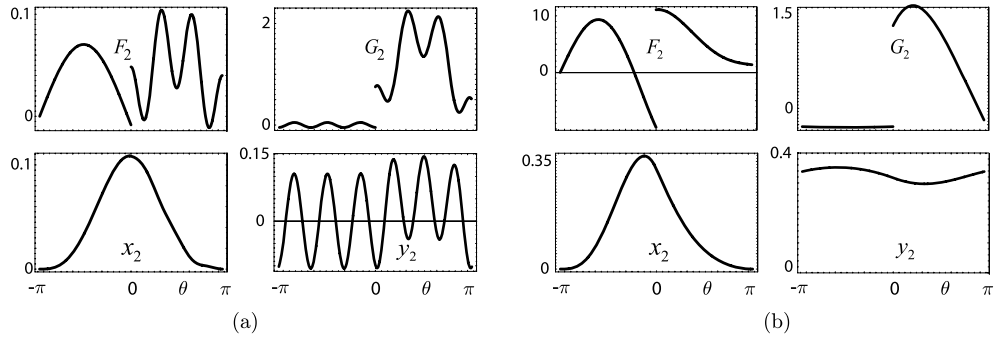

Fig. 4 Nonsmooth excitations of the second-order perturbation equations (31) and relevant responses; (**a**) first mode; (**b**) second mode

Finally, using previous results and solving (31), with the relevant boundary conditions, we find that:

$$x_2 = \begin{cases} A_2^+ \cos\theta + B_2^+ \sin\theta + \hat{x}_2^+, & \theta \in [0, \pi], \\ A_2^- \cos\theta + B_2^- \sin\theta + \hat{x}_2^-, & \theta \in [-\pi, 0], \end{cases}$$

$$y_2 = \begin{cases} C_2^+ \cos(\lambda\theta) + D_2^+ \sin(\lambda\theta) + \hat{y}_2^+, \\ \quad \theta \in [0, \pi], \\ C_2^- \cos(\lambda\theta) + D_2^- \sin(\lambda\theta) + \hat{y}_2^-, \\ \quad \theta \in [-\pi, 0], \end{cases} \tag{34}$$

where A_2's, B_2's, C_2's and D_2's constants are reported in Appendix B together with the particular solutions $\hat{x}_2$'s and $\hat{y}_2$'s. The forcing functions in (31) and the responses (34) are plotted in Fig. 4.

By summarizing and returning to the true time t, the x-NNM at the ε^2-order, reads:

$$\begin{aligned} \mathbf{q}(t) = \mathbf{u}_x \Bigg[& a \sin\Omega_x t + \varepsilon \Bigg(A_1^{\pm} \cos\Omega_x t + B_1^{\pm} \sin\Omega_x t \\ & \mp \frac{a c_{xx}}{4\omega_x^2} \Omega_x t \cos\Omega_x t \Bigg) \\ & + \varepsilon^2 \big(A_2^{\pm} \cos\Omega_x t + B_2^{\pm} \sin\Omega_x t \\ & \mp \hat{x}_2^{\pm}(\Omega_x t, \Omega_y t) \big) \Bigg] \\ & + \mathbf{u}_y \Bigg[\varepsilon \Bigg(C_1^{\pm} \cos\Omega_y t + D_1^{\pm} \sin\Omega_y t \\ & \pm \frac{a c_{yx} H[\Omega_x t]}{\omega_x^2(\lambda^2 - 1)} \sin\Omega_x t \Bigg) \\ & + \varepsilon^2 \big(C_2^{\pm} \cos\Omega_y t + D_2^{\pm} \sin\Omega_y t \\ & \mp \hat{y}_2^{\pm}(\Omega_x t, \Omega_y t) \big) \Bigg] \end{aligned} \tag{35}$$

where:

$$\Omega_\alpha = \omega_\alpha \big(1 + \varepsilon\mu_1 + \varepsilon^2 \mu_2 \big), \quad \alpha = x, y \tag{36}$$

are the nonlinear frequencies and the upper sign must be taken when $t \in [0, \pi/\Omega_x]$ and the lower when $t \in [-\pi/\Omega_x, 0]$. It should be noted that both frequencies, the active ω_x and the passive ω_y, are modified by the same factor, which depends on the damage intensity ε and is independent of a, as expected for a piecewise oscillator and in accordance with [28, 29].

3.3 Stability analysis

The stability of the periodic solution so far determined is analyzed through Floquet's theory. By denoting by $\mathbf{q}_s(t) = \mathbf{q}_s(t + 2\pi/\Omega_x)$ the steady-state periodic solution and by $\tilde{\mathbf{q}}(t)$ its perturbation, with $\|\tilde{\mathbf{q}}\| \ll \|\mathbf{q}_s\|$,

$$\mathbf{q}(t) = \mathbf{q}_s(t) + \tilde{\mathbf{q}}(t) \tag{37}$$

is posed in the equation of motion. Since

$$H\big[\mathbf{a}^T \mathbf{q}\big] = \big[\mathbf{a}^T \mathbf{q}_s\big] + \delta\big[\mathbf{a}^T \mathbf{q}_s\big] \mathbf{a}^T \tilde{\mathbf{q}} + \cdots \tag{38}$$

the *variational equation*, linearized in $\tilde{\mathbf{q}}(t)$, reads

$$\mathbf{M}\ddot{\tilde{\mathbf{q}}} + \big(\mathbf{K}_0 - \varepsilon H\big[\mathbf{a}^T \mathbf{q}_s\big] \mathbf{K}_2 \big) \tilde{\mathbf{q}} = \mathbf{0} \tag{39}$$

having taken into account that $\delta[\mathbf{a}^T \mathbf{q}_s]\mathbf{q}_s$ does not furnish contribution to the solution. The variational equation is an o.d.e. with periodic coefficients varying with a nonsmooth law. According to Floquet' theory, the stability of $\mathbf{q}_s(t)$ is governed by the characteristic multipliers γ of the monodromy matrix, i.e.,

the matrix of a fundamental system of solutions evaluated at $t = 2\pi/\Omega_x$, obtained by imposing linearly independent initial conditions $\tilde{q}_i(0) = \delta_{ij}$, $\dot{\tilde{q}}_i(0) = 0$ and $\tilde{q}_i(0) = 0$, $\dot{\tilde{q}}_i(0) = \delta_{ij}$ $(j = 1, 2)$, with δ_{ij} the Kronecher symbol. If all the magnitude of the characteristic multipliers γ_k $(k = 1, \ldots, 4)$ are smaller than one the periodic solution is asymptotically stable, if the magnitude of only one characteristic multipliers γ_k is larger than one, it is unstable. Here, the monodromy matrix has been obtained by numerically integrating the variational equation. Analytical solutions have been left for future investigations.

4 Numerical solution of nonlinear normal modes

To verify the approximation of the perturbative solution and investigate the global dynamics of some cases of the piecewise system, a computational approach has been developed. In searching the periodic solutions, it is convenient to rewrite the system (6) in the phase space:

$$\dot{\mathbf{x}} = \mathbf{A}(\mathbf{x}; \varepsilon)\mathbf{x}, \qquad \mathbf{x}(0) = \mathbf{x}_0 \tag{40}$$

where $\mathbf{x} = (\mathbf{q}, \dot{\mathbf{q}})^T$. Periodic solutions $\hat{\mathbf{x}}(t; \mathbf{x}_0)$ of period T are found as roots of the following equations:

$$\mathbf{x}(T; \mathbf{x}_0) - \mathbf{x}_0 = \mathbf{0}, \qquad \mathbf{A}(\mathbf{x}; \varepsilon)\mathbf{x}_0 \cdot (\mathbf{x} - \mathbf{x}_0) = 0 \tag{41}$$

where the last condition fixes the phase along the orbit and represents the Poincaré phase condition. From a computational point of view, the procedure valid for generic autonomous systems can be simplified for piecewise linear systems. Because of the conservative character of the latter, it is possible to limit the research of the initial conditions $\mathbf{x}_0$ in the configuration space along the isoenergetic curves $\mathcal{C}(\varepsilon) = \{\mathbf{q} \mid 1/2\mathbf{q}^T\mathbf{K}(\mathbf{q}; \varepsilon)\,\mathbf{q} = \mathcal{H}\}$. Moreover, since for each solution $\hat{\mathbf{x}}(t; \mathbf{x}_0)$ of (40) the similarity properties hold [28], namely:

$$\hat{\mathbf{x}}(t; \alpha\mathbf{x}_0) = \alpha\hat{\mathbf{x}}(t; \mathbf{x}_0) \tag{42}$$

it is possible to restrict the initial conditions to one isoenergy curve only, e.g., $\mathcal{H}_0$. This circumstance removes the arbitrariness of the initial phase, so that the independent parameters are only two, namely a configuration parameter and the period T. In Fig. 2, the isoenergetic curve $\mathcal{H}_0$ is shown. This curve is of smooth type, since in correspondence of the discontinuity boundary $\eta = 0$ (dashed line in Fig. 2), the two curves relative to the damaged and the undamaged system joint with the same tangent because of continuity of the restoring bilinear force. Computational efficiency is improved when the periodicity gap $\Delta(T, \mathbf{x}_0) := \mathbf{x}(T; \mathbf{x}_0) - \mathbf{x}_0$ is projected onto the tangent to the level set $\mathcal{H}_0$ ($\mathbf{w}_1$ vector in Fig. 2) and on the direction of the Hamiltonian vector field $\mathbf{A}(\mathbf{x}; \varepsilon)\mathbf{x}$ ($\mathbf{w}_2$ vector in Fig. 2).

5 Numerical investigation

A parametric analysis of the NNMs of a sample system is performed for different values of the damage parameter ε. The undamaged system is characterized by the following values of parameters $\tilde{m}_i = 0.5$, $\tilde{I}_i = 0.5$, $\tilde{k}_i = 1$. The linear frequencies and the associated eigenvectors normalized to the mass matrix are respectively:

$$\omega_x = 1.171, \qquad \omega_y = 6.828,$$
$$\mathbf{u}_x = \begin{pmatrix} 1.082 \\ 1.530 \end{pmatrix}, \qquad \mathbf{u}_y = \begin{pmatrix} -2.613 \\ 3.695 \end{pmatrix}. \tag{43}$$

The nonlinear frequencies furnished by the ε^2-order asymptotic expression (36) are plotted in Fig. 5 versus the damage parameter, here extended up to the extremum value $\varepsilon = 1$. As expected, both frequencies monotonically decrease with ε. These analytical results were compared with results obtained following the numerical procedure based on the Poincaré map approach. The percentage errors between the numerical and ε- or ε^2-order perturbation frequencies are reported in Table 1 for both modes. Although the accuracy of the perturbation solution naturally deteriorates for increasing ε, it is still good for large values of the parameter. It is noted that for any values of ε, the approximation of the first frequency is better than that of the second frequency. Moreover, the second-order approximation remarkably reduces the error.

A comparison between perturbative and numerical time-histories of the normal coordinates was then performed. Figure 6 shows the first-order, second-order, and numerical laws $x(\theta)$ and $y(\theta)$ when $\varepsilon = 0.25$ for both modes. The $x(\theta)$ law is well approximated already by the first-order perturbation solution, whereas the $y(\theta)$ law is well averaged approximated by the per-

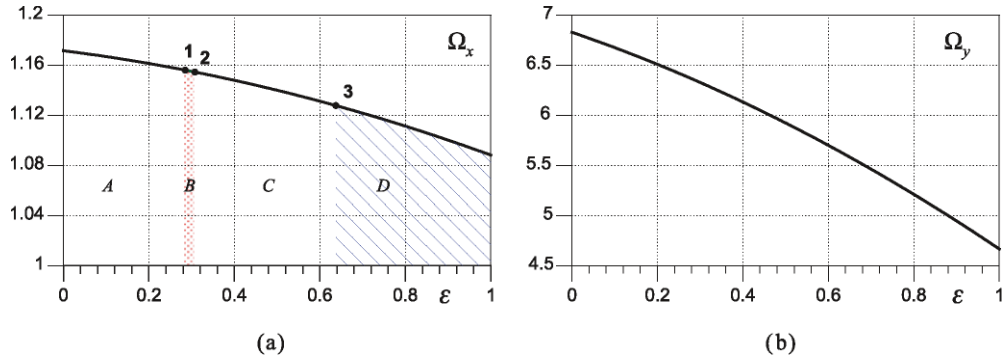

Fig. 5 Variation of the (**a**) first- and (**b**) second-order perturbation frequencies versus damage parameter ε

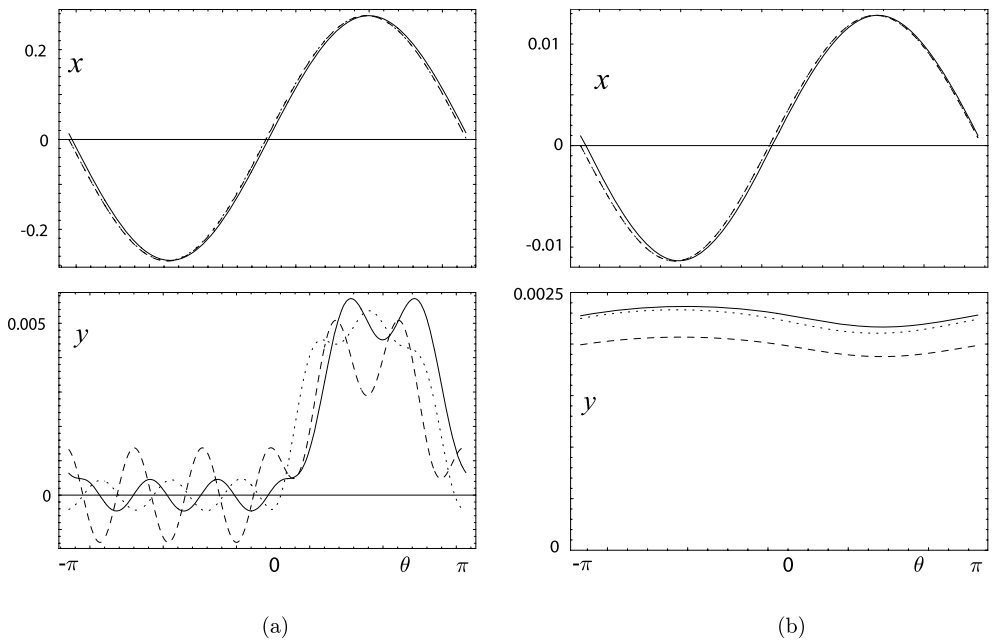

Fig. 6 Time-histories of the normal coordinates when $\varepsilon = 0.25$; (**a**) first-mode, (**b**) second-mode; *dashed line* ε-order, *dotted line* ε^2-order, *solid line* numerical

Table 1 Percentage error Δ_k between numerical and kth-order perturbation frequencies

ε	1st mode		2nd mode	
	$\Delta_1\%$	$\Delta_2\%$	$\Delta_1\%$	$\Delta_2\%$
0.25	0.25	0.03	0.84	0.16
0.30	0.50	0.18	1.29	0.28
0.50	1.65	0.76	4.45	1.43

turbation solution. In particular, the approximation improves with the order of the asymptotic expansion.

The $x(\theta)$ and $y(\theta)$ laws are the parametric equations of a curve, which represents the projection on the configuration space of the modal line belonging to the phase space. The modal lines associated with the ε-order time-histories of Fig. 6 are plotted in Fig. 7. It is observed that the perturbation method furnishes two slightly different curves for each half-cycle (two-way modal lines), instead of a unique open curve, since in the two intervals $[-\pi, 0]$ and $[0, \pi]$, they are described by different parametric laws. However, since the curves are very close to each other, it is possible to refer to only one of

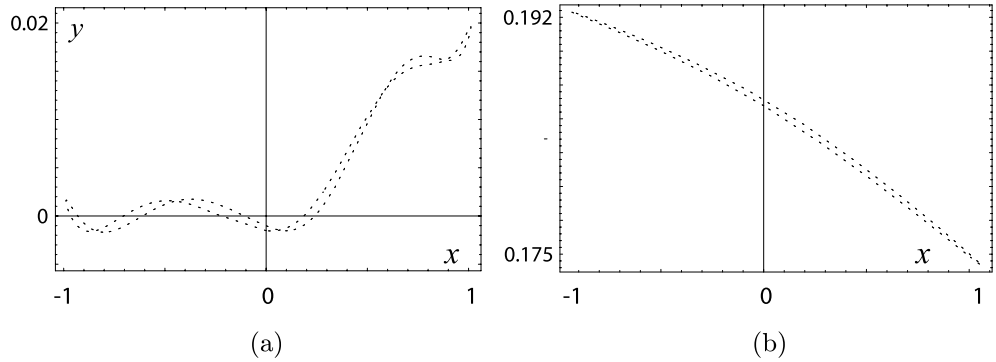

Fig. 7 Two-wise ε-order modal lines in the normal coordinate space when $\varepsilon = 0.25$; (**a**) first-mode, (**b**) second-mode

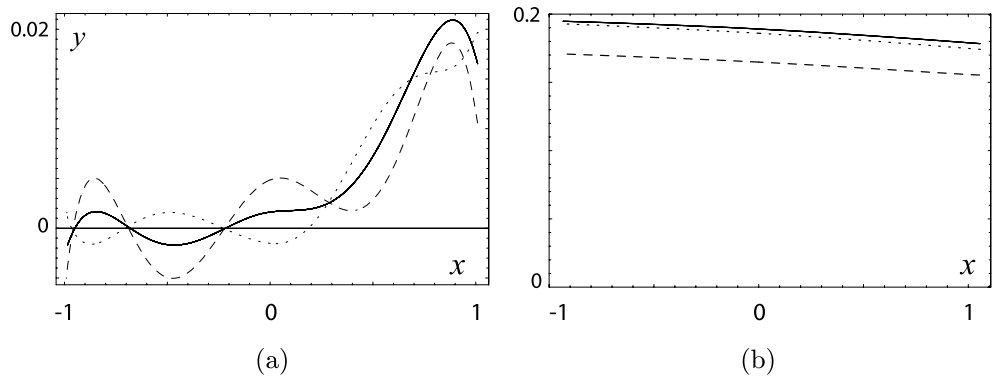

Fig. 8 Modal lines in the normal coordinates space when $\varepsilon = 0.25$; (**a**) first-mode, (**b**) second-mode; *dashed line* ε-order, *dotted line* ε^2-order, *solid line* numerical

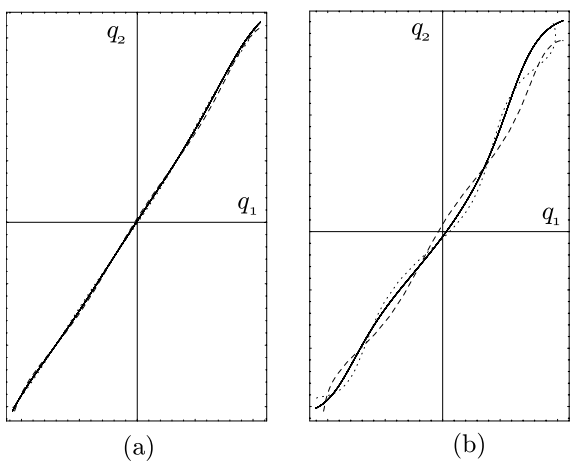

Fig. 9 Modal lines in the configuration-space for the first-mode; (**a**) $\varepsilon = 0.25$; (**b**) $\varepsilon = 0.50$; *dashed line* ε-order, *dotted line* ε^2-order, *solid line* numerical

them. The associated modal lines, where the y-scale is magnified with respect to the x-scale, are plotted in Fig. 8.

Due to nonlinearities, the linear x-mode line is slightly bent in the first mode, and remarkably shifted in the second mode. Both effects are fairly well captured by the perturbation method. When the curves are plotted (in the same scale) in Lagrangian coordinates, they assume the shapes shown in Figs. 9a and 10a, while in Figs. 9b and 10b, the curves are drawn for $\varepsilon = 0.50$. Comparison among the first and second modal curves highlights some differences, namely: (a) the first modal curves are slightly bent in several waves, while the second modal curves are nearly straight; (b) the second modal curves undergo a more marked drift than the first modal curves, with differences increasing with ε; (c) the shape of the first modal curve depends on ε, while the second is independent of it. The perturbation solution throws light on such be-

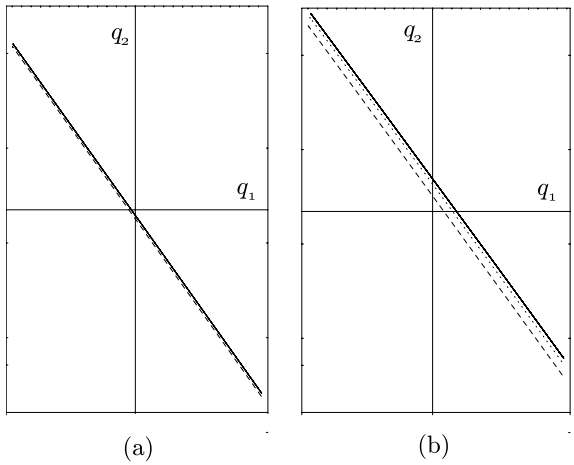

Fig. 10 Modal lines in the configuration-space for the second-mode; (**a**) $\varepsilon = 0.25$; (**b**) $\varepsilon = 0.50$; *dashed line* ε-order, *dotted line* ε^2-order, *solid line* numerical

haviors. First of all, the occurrence of drift is explained by the ε-order perturbation equations, from which it emerges that the forcing term (see (20_2)) consists of an intermittent signal having constant sign (Figs. 4 and 5). Moreover, since nonlinear forces consist of self-equilibrated couples acting at hinge 2 (namely, the gap of the internal moment), nonlinearities in the $\mathbf{u}_y$-mode are stronger than those in the $\mathbf{u}_x$-mode due to larger relative rotations. This circumstance entails that the contribution of $\mathbf{u}_y$ to the first NNM is greater than the contribution of $\mathbf{u}_x$ to the second NNM, thus explaining why the latter remains almost linear. In addition, the perturbation solution (see (35)) shows that the passive mode participates in the NNM with two contributions: a forced motion at the basic frequency, and a free motion at the (slightly modified) proper frequency, which is higher than the basic frequency in the first NNM and smaller than the basic frequency in the second NNM as is evidenced in Fig. 6, thus explaining the presence (or absence) of waves in the modal lines.

Stability analysis of NNMs is then performed. Asymptotic analysis of the first mode shows that (Fig. 5a): at $\varepsilon \simeq 0.28$ a flip critical condition arises, i.e., two eigenvalues γ_i $(i = 1, 2)$ of the monodromy matrix leave the unit circle at $\mathrm{Re}(\gamma_i) = -1$; at $\varepsilon \simeq 0.31$, they return to the unit circle always with $\mathrm{Re}(\gamma_i) = -1$; at $\varepsilon \simeq 0.64$ another critical condition occurs, in particular, two eigenvalues leave the unit circle with $\mathrm{Re}(\gamma_i) = 1$ (divergence bifurcation). Consequently, in the intervals A and C of Fig. 5a, the first NNM is stable, while in the intervals B and D are unstable. The second mode is found to be stable in the whole range of the parameter ε. The stability analysis was repeated following the numerical Poincaré map approach. It confirmed that the second mode is always stable while it was found that at $\varepsilon \simeq 0.72$ (i.e., at a slightly different value of the perturbation result), the first mode encounters a turning point and is unstable in the interval [0.28–0.31] coincident to that evidenced by the perturbation solution. In particular in the B region, additional substantially different solutions of period approximately double those of the first mode were furnished by the numerical analysis; it was demonstrated that in this region the system exhibits superabundant modes. Their shape is markedly different from the basic shape and they are shown in Fig. 11, when $\varepsilon = 0.3$.

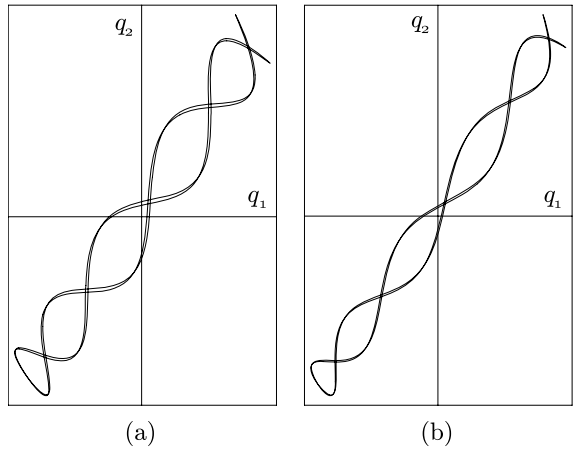

Fig. 11 Superabundant normal modes when $\varepsilon = 0.3$

6 Conclusions

A piecewise two degrees-of-freedom system, representative of a cracked beam was analyzed. It belongs to the class of nonsmooth systems that are candidates to exhibit a number of nonlinear normal modes greater than the degrees of freedom. An analytical solution, up to ε^2-order, was obtained by an enhanced Lindstedt–Poincaré method, which makes it possible to give a closed form expression to the modification of frequencies and mode shapes. Differently from the classical approach, valid for smooth systems, the complementary solution of the passive coordinate equations must

here be taken into account, in order to satisfy continuity and periodicity of motion. As a result, both passive and active frequencies, modified by the same damage-dependent factor, contribute to the motion although they are incommensurable. Moreover, secular terms appear in the solution that do not diverge in the finite period of motion. Results of the stability analysis show that while the second mode is always stable, the first mode is unstable for some values of the damage parameter. Numerical results, obtained by a Poincaré map approach, confirm the perturbation results and also show the existence of superabundant normal modes which arise in the unstable interval of the first mode.

Acknowledgements This work was partially supported under the FY 2005-2007 PRIN Grant "modeling and experimental tests of the dynamic behavior of flexible structures" from the Italian Ministry of Education, University, and Scientific Research.

Appendix A: Higher-order solutions involving the Dirac function

Although the perturbation solution, here developed up-to ε^2-order, does not involve the Dirac function, nor its derivatives, it is worth discussing how to deal with higher-order perturbation equations, where such a generalized function in contrast appears. The equations to solve have the following form:

$$\begin{cases} \ddot{x} + \omega^2 x = \delta[e_0 \sin\theta] F(\theta) + \delta'[e_0 \sin\theta] G(\theta) \\ \qquad\qquad + \cdots + R(\theta), \\ x(-\pi^+) = x(\pi^+), \qquad \dot{x}(-\pi^+) = \dot{x}(\pi^+) \end{cases} \tag{44}$$

where, by accounting for (15), $\eta_0 = e_0 \sin\theta$, $e_0 > 0$, has been posed. Moreover, $F(\theta)$, $G(\theta)$, and $R(\theta)$ are 2π-periodic known functions, with $R(\theta)$ collecting all the no-δ terms. All these functions are generally discontinuous at $\theta = k\pi$, $k = 0, \pm 1, \pm 2, \ldots$, i.e., they are of the type plotted in Fig. 4. Derivatives of δ higher than first also appear, but δ' is sufficient to illustrate the procedure. It should be noted that since the forcing δ-terms represent a train of (generalized) impulses applied at $\theta = k\pi$, the periodicity conditions, (19), must be changed as in (44_2); in contrast, no continuity is enforced at $\theta = 0$ (see 18), since (44_1) holds in the $(-\infty, +\infty)$ interval.

By using the Duhamel integral, and writing the response to the unitary impulse as $h(\theta) := H(\theta) \times \sin(\omega\theta)/\omega$, the general solution to (44), for $\theta \in [-\pi^+, +\pi^+]$, reads

$$\begin{aligned} x(\theta) = {} & A\cos(\omega\theta) + B\sin(\omega\theta) + x_R(\theta) \\ & + \frac{1}{\omega}\int_{-\pi^+}^{0} \delta[e_0 \sin\theta] F(\tau) H[\theta - \tau] \\ & \times \sin\big(\omega(\theta - \tau)\big)\, d\tau \\ & + \frac{1}{\omega}\int_{-\pi^+}^{\theta} \delta'[e_0 \sin\theta] G(\tau) H[\theta - \tau] \\ & \times \sin\big(\omega(\theta - \tau)\big)\, d\tau \end{aligned} \tag{45}$$

where $x_R(\theta)$ is the answer to $R(\theta)$, and A and B are arbitrary constants to be determined via the periodicity conditions along the lines already discussed (see Sect. 3.1). By using known properties of the Dirac function, it is found that

$$\begin{aligned} \int_{-\infty}^{+\infty} \delta[\sin\theta] f(\theta)\, d\theta &= \sum_{k=-\infty}^{+\infty} f(k\pi), \\ \int_{-\infty}^{+\infty} \delta'[\sin\theta] f(\theta)\, d\theta &= -\sum_{k=-\infty}^{+\infty} (-1)^k \dot{f}(k\pi) \end{aligned} \tag{46}$$

where the second integral has been obtained via integration by parts. With (46), the general solution (45) becomes:

$$\begin{aligned} x(\theta) = {} & A\cos(\omega\theta) + B\sin(\omega\theta) + x_R(\theta) \\ & + \frac{1}{\omega e_0}\Big\{ H[\theta] F\big(0^{\pm}\big) \sin(\omega\theta) \\ & + H[\theta - \pi] F\big(\pi^{\pm}\big) \sin\big(\omega(\theta - \pi)\big) \Big\} \\ & + \frac{1}{\omega e_0^2}\Big\{ H[\theta] \big(G\big(0^{\pm}\big)\omega\cos(\omega\theta) \\ & - G'\big(0^{\pm}\big)\sin(\omega\theta) \big) \\ & + H[\theta - \pi] \big(G\big(\pi^{\pm}\big) \big) \omega\cos\big(\omega(\theta - \pi)\big) \\ & - G'\big(\pi^{\pm}\big)\sin\big(\omega(\theta - \pi)\big) \Big\}. \end{aligned} \tag{47}$$

Equation (47) expresses a component of motion $x(\theta)$ as the sum of the answers to prescribed *jumps of velocities*, proportional to $F(k\pi)$, and *jumps of displacements*, proportional to $G(k\pi)$. Both kinds of jumps are approximations of changes of state really occurring in short-time intervals $\Delta\theta_k = O(\varepsilon)$ (see Fig. 12).

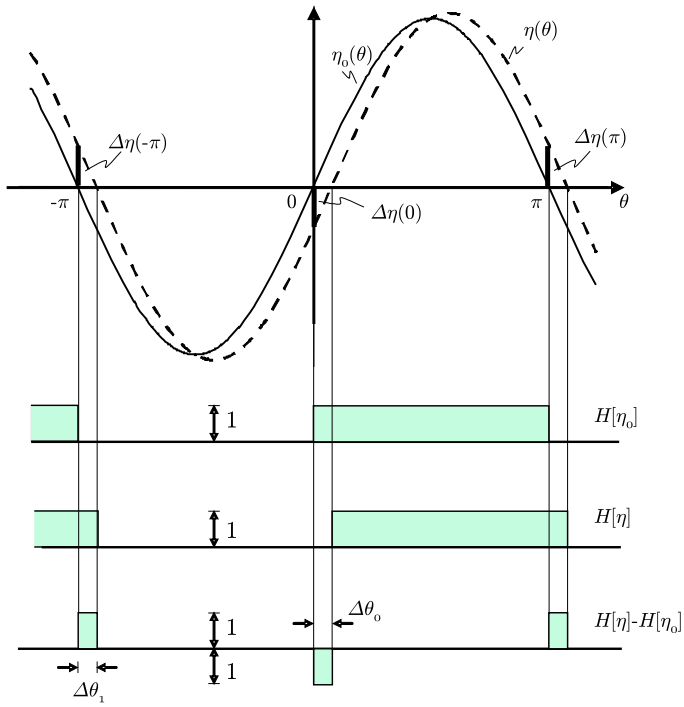

Fig. 12 Perturbation of $H[\eta(\varepsilon)]$ around $\eta_0 = e_0 \sin\theta$, leading to short-time excitations

These intervals both follow ($\Delta\theta_k > 0$) or precede ($\Delta\theta_k < 0$) the instants $\theta = k\pi$, at which jumps have been lumped, as consequence of having expanded $H[\eta(\varepsilon)]$ by the series (12). The sign of $\Delta\theta_k$ depends on the sign of the perturbation $\Delta\eta(k\pi)$, hence, by the sign of its leading part $\eta_1(k\pi)$ (namely, $\Delta\theta_0 > 0$ if $\eta_1(0) < 0$, $\Delta\theta_1 > 0$ if $\eta_1(\pi) > 0$, and vice versa).

This interpretation of the mechanical phenomenon permits resolving the mathematical ambiguities present in (47), due to the discontinuity of F and G functions. Accordingly, the F- and G-values at 0^+ (and π^+) will be taken if $\Delta\theta_0 > 0$ (and $\Delta\theta_1 > 0$) and the values at 0^- (and π^-) will be taken if $\Delta\theta_0 < 0$ (and $\Delta\theta_1 < 0$).

Appendix B: Solution to the second-order perturbative equations

The constants appearing in (34) assume the following expressions:

$$A_2^+ = \frac{a\pi(3(\lambda^2-1)c_{xx}^2 + 8c_{xy}^2)}{32(\lambda^2-1)\omega_1^4},$$
$$B_2^+ = -\frac{a(8\cot(\frac{\pi\lambda}{2})c_{xy}^2 + \pi\lambda((-2+\pi^2)(\lambda^2-1)^2c_{xx}^2 - 4(\lambda^2-5)c_{xy}^2))}{32\pi\lambda(\lambda^2-1)^2\omega_1^4}, \tag{48}$$

$$A_2^- = \frac{a(16\cot(\frac{\pi\lambda}{2})c_{xy}^2 + \pi\lambda(\lambda^2-1)(5(\lambda^2-1)c_{xx}^2 + 8c_{xy}^2))}{32\lambda(\lambda^2-1)^2\omega_1^4},$$
$$B_2^- = -\frac{a(8\cot(\frac{\pi\lambda}{2})c_{xy}^2 + \pi\lambda(\lambda^2-1)((2+\pi^2)(\lambda^2-1)c_{xx}^2 + 4c_{xy}^2))}{32\pi\lambda(\lambda^2-1)^2\omega_1^4}, \tag{49}$$

$$C_2^+ = \frac{a\csc^2(\frac{\pi\lambda}{2})(2\pi(\lambda^2-1)\cos(\pi\lambda)c_{xx}\lambda^2+\sin(\pi\lambda)((\lambda^2+7)c_{xx}-8c_{yy})\lambda-2\pi(\lambda^2-1)c_{yy})c_{xy}}{32(\lambda^3-\lambda)^2\omega_1^4},$$
$$D_2^+ = \frac{a(2\pi(\lambda^2-1)\cot(\pi\lambda)c_{xx}\lambda^2+((\lambda^2+7)c_{xx}-8c_{yy})\lambda+2\pi(\lambda^2-1)\csc(\pi\lambda)c_{yy})c_{xy}}{16(\lambda^3-\lambda)^2\omega_1^4}, \tag{50}$$

$$C_2^- = -\frac{a\csc^2(\frac{\pi\lambda}{2})}{32\lambda^3(\lambda^2-1)^2\omega_1^4}\big(2\pi(\lambda^2-1)\cos(\pi\lambda)c_{xx}\lambda^3-2\pi(\lambda^2-1)(2\lambda^2c_{xx}-c_{yy})\lambda$$
$$+\sin(\pi\lambda)\big(2(5\lambda^2-1)c_{yy}-\lambda^2(\lambda^2+7)c_{xx}\big)\big)c_{xy}, \tag{51}$$

$$D_2^- = \frac{a(-c_{xx}\lambda^4+2\pi(\lambda^2-1)\cot(\pi\lambda)c_{xx}\lambda^3-7c_{xx}\lambda^2+10c_{yy}\lambda^2+2\pi(\lambda^2-1)\csc(\pi\lambda)c_{yy}\lambda-2c_{yy})c_{xy}}{16\lambda^3(\lambda^2-1)^2\omega_1^4}.$$

The particular solutions present in the same equations are

$$\hat{x}_2^+ = \frac{\pi c_{xx}^2}{32\omega_1^4}a\cos\theta+\frac{\pi\lambda(\lambda^2-1)((\lambda^2-1)c_{xx}^2+2c_{xy}^2)-4\cot(\frac{\pi\lambda}{2})c_{xy}^2}{16\pi\lambda(\lambda^2-1)^2\omega_1^4}a\sin\theta$$
$$+\frac{\cot(\frac{\pi\lambda}{2})c_{xy}^2}{2\lambda(\lambda^2-1)^2\omega_1^4}a\cos\lambda\theta+\frac{c_{xy}^2}{2\lambda(\lambda^2-1)^2\omega_1^4}a\sin\lambda\theta+\frac{\pi c_{xx}^2}{16\omega_1^4}a\theta\sin\theta$$
$$-\frac{\pi\lambda(\lambda^2-1)((\lambda^2-1)c_{xx}^2+2c_{xy}^2)-4\cot(\frac{\pi\lambda}{2})c_{xy}^2}{8\pi\lambda(\lambda^2-1)^2\omega_1^4}a\theta\cos\theta-\frac{c_{xx}^2}{32\omega_1^4}a\theta^2\sin\theta, \tag{52}$$

$$x_2^- = -\frac{\pi c_{xx}^2}{32\omega_1^4}a\cos\theta-\frac{4\cot(\frac{\pi\lambda}{2})c_{xy}^2+\pi\lambda(\lambda^2-1)((\lambda^2-1)c_{xx}^2+2c_{xy}^2)}{16\pi\lambda(\lambda^2-1)^2\omega_1^4}a\sin\theta$$
$$+\frac{4\cot(\frac{\pi\lambda}{2})c_{xy}^2+\pi\lambda(\lambda^2-1)((\lambda^2-1)c_{xx}^2+2c_{xy}^2)}{8\pi\lambda(\lambda^2-1)^2\omega_1^4}a\theta\cos\theta-\frac{\pi c_{xx}^2}{16\omega_1^4}a\theta\sin\theta-\frac{c_{xx}^2}{32\omega_1^4}a\theta^2\sin\theta, \tag{53}$$

$$\hat{y}_2^+ = \frac{\pi c_{xx}c_{xy}}{4(\lambda^2-1)\omega_1^4}a\cos\theta+\frac{((\lambda^2-5)c_{xx}+4c_{yy})c_{xy}}{4(\lambda^2-1)^2\omega_1^4}a\sin\theta+\frac{\cot(\frac{\pi\lambda}{2})(\lambda^2c_{xx}-2c_{yy})c_{xy}}{16\lambda^3(\lambda^2-1)\omega_1^4}a\cos\lambda\theta$$
$$+\frac{(\lambda^2c_{xx}-2c_{yy})c_{xy}}{16\lambda^3(\lambda^2-1)\omega_1^4}a\sin\lambda\theta-\frac{c_{xx}c_{xy}}{4(\lambda^2-1)\omega_1^4}a\theta\cos\theta-\frac{(\lambda^2c_{xx}-2c_{yy})c_{xy}}{8\lambda^2(\lambda^2-1)\omega_1^4}a\theta\cos\lambda\theta$$
$$+\frac{\cot(\frac{\pi\lambda}{2})(\lambda^2c_{xx}-2c_{yy})c_{xy}}{8\lambda^2(\lambda^2-1)\omega_1^4}a\theta\sin\lambda\theta, \tag{54}$$

$$y_2^- = \frac{\cot(\frac{\pi\lambda}{2})c_{xx}c_{xy}}{16(\lambda^3-\lambda)\omega_1^4}a\cos\lambda\theta-\frac{c_{xx}c_{xy}}{16(\lambda^3-\lambda)\omega_1^4}a\sin\lambda\theta+\frac{c_{xx}c_{xy}}{8(\lambda^2-1)\omega_1^4}a\theta\cos\lambda\theta$$
$$+\frac{\cot(\frac{\pi\lambda}{2})c_{xx}c_{xy}}{8(\lambda^2-1)\omega_1^4}a\theta\sin\lambda\theta. \tag{55}$$

References

1. Rosenberg, R.M.: On normal vibrations of a general class of nonlinear dual-mode systems. J. Appl. Mech. **29**, 7–14 (1962)
2. Rosenberg, R.M.: Nonsimilar normal mode vibrations of nonlinear systems having two degrees of freedom. J. Appl. Mech. **31**, 7–14 (1964)
3. Rosenberg, R.M.: On nonlinear vibration of systems with many degrees of freedom. Adv. Appl. Mech. **9**, 155–242 (1966)
4. Shaw, S.W., Pierre, C.: Nonlinear normal modes and invariant manifolds. J. Sound Vib. **150**(1), 170–173 (1991)
5. Shaw, S.W., Pierre, C.: Normal modes for non-linear vibratory systems. J. Sound Vib. **1**, 85–124 (1993)
6. Shaw, S.W., Pierre, C.: Normal modes of vibration for nonlinear continuous systems. J. Sound Vib. **169**(3), 319–347 (1994)
7. Rand, R.: A direct method for non-linear normal modes. Int. J. Non-Linear Mech. **9**, 363–368 (1974)
8. Rand, R., Pak, C., Vakakis, A.: Bifurcation of nonlinear normal modes in a class of two-degree-of-freedom-systems. Acta Mech. **3**, 129–145 (1992)
9. Vakakis, A.F., Manevitch, L.I., Mikhlin, Y.V., Pilipchuck, V.N., Zevin, A.A.: Normal Modes and Localizations in Nonlinear Systems. Wiley, New York (1996)
10. Nayfeh, A.H.: Direct methods for constructing nonlinear normal modes of continuous systems. J. Vib. Control **1**(4), 389–430 (1995)
11. Nayfeh, A.H., Chin, C., Nayfeh, S.A.: On nonlinear normal modes of systems with internal resonance. J. Vib. Acoust. **118**, 340–345 (1996)
12. Nayfeh, A.H.: Nonlinear Interactions. Analytical, Computational and Experimental Methods. Wiley, New York (2000)
13. Nayfeh, A.H., Nayfeh, S.A.: On nonlinear modes of continuous systems. J. Vib. Acoust. **116**, 129–136 (1994)
14. Lacarbonara, W., Camillacci, R.: Nonlinear normal modes of structural systems via asymptotic approach. Int. J. Solids Struct. **41**, 5565–5594 (2004)
15. Anand, G.V.: Natural modes of coupled non-linear systems. Int. J. Non-Linear Mech. **7**, 81–91 (1972)
16. Pak, C.H.: On the stability behaviour of bifurcated normal modes in coupled nonlinear systems. J. Appl. Mech. **56**, 155–161 (1989)
17. Vakakis, A.F.: Non-linear normal modes and their applications in vibration theory: an overview. Mech. Syst. Signal Process. **11**, 3–22 (1997)
18. Johnson, T.L., Rand, R.: On the existence and bifurcation of minimal normal modes. Int. J. Non-Linear Mech. **14**, 1–12 (1979)
19. Gourdon, E., Lamarque, C.H.: Energy pumping for a larger span of energy. J. Sound Vib. **286**, 1–9 (2005)
20. Lee, Y.S., Kerschen, G., Vakakis, A.F., Panagopoulos, P.N., Bergman, L.A., McFarland, D.M.: Complicated dynamics of a linear oscillator with a light, essentially nonlinear attachment. Physica D **204**, 41–69 (2005)
21. Den Hartog, J.P., Heiles, R.M.: Forced vibration in nonlinear systems with various combinations of linear springs. J. Appl. Mech. **3**, 127–30 (1936)
22. Bogoliubov, N.N., Mitropolsky, Y.A.: Asymptotic Methods in the Theory of Nonlinear Oscillations. Gordon and Breach, New York (1961)
23. Chati, M., Rand, R., Mukherjee, S.: Modal analysis of a cracked beam. J. Sound Vib. **207**(2), 249–270 (1997)
24. Natsiavas, S.: Stability and bifurcation analysis for oscillators with motion limiting constraints. J. Sound Vib. **141**, 97–102 (1990)
25. Natsiavas, S.: Dynamics of multiple-degree-of-freedom oscillators with colliding components. J. Sound Vib. **165**, 439–453 (1993)
26. Chen, S., Shaw, S.W.: Normal modes for piecewise linear vibratory systems. Nonlinear Dyn. **10**, 135–163 (1996)
27. Jiang, D., Pierre, C., Shaw, S.W.: Large-amplitude nonlinear normal modes of piecewise linear systems. J. Sound Vib. **272**, 869–891 (2004)
28. Zuo, L., Currier, A.: Non-linear and complex modes of conewise linear systems. J. Sound Vib. **174**, 289–313 (1994)
29. Andreaus, U., Casini, P., Vestroni, F.: Non-linear dynamics of a cracked cantilever beam under harmonic excitation. Int. J. Non-Linear Mech. **42**(3), 566–575 (2007)
30. Casini, P., Vestroni, F.: Nonstandard bifurcations in mechanical systems with multiple discontinuity boundaries. Nonlinear Dyn. **35**, 41–54 (2004)